

Axion wind detection with the homogeneous precession domain of superfluid helium-3

Christina Gao,^{1,2,3} William Halperin,⁴ Yonatan Kahn,^{1,2} Man
Nguyen,⁴ Jan Schütte-Engel,^{1,2} and John William Scott⁴

¹*Department of Physics, University of Illinois Urbana-Champaign, Urbana, IL 61801, USA*

²*Illinois Center for Advanced Studies of the Universe,*

University of Illinois Urbana-Champaign, Urbana, IL 61801, USA

³*Theoretical Physics Division, Fermi National Accelerator Laboratory, Batavia, IL 60510, USA*

⁴*Department of Physics and Astronomy, Northwestern University, Evanston, IL 60208, USA*

(Dated: September 27, 2022)

Axions and axion-like particles may couple to nuclear spins like a weak oscillating effective magnetic field, the “axion wind.” Existing proposals for detecting the axion wind sourced by dark matter exploit analogies to nuclear magnetic resonance (NMR) and aim to detect the small transverse field generated when the axion wind resonantly tips the precessing spins in a polarized sample of material. We describe a new proposal using the homogeneous precession domain (HPD) of superfluid ³He as the detection medium, where the effect of the axion wind is a small shift in the precession frequency of a large-amplitude NMR signal. We argue that this setup can provide broadband detection of multiple axion masses simultaneously, and has competitive sensitivity to other axion wind experiments such as CASPEr-Wind at masses below 10⁻⁷ eV by exploiting precision frequency metrology in the readout stage.

Axions and axion-like particles (ALPs) (denoted a) are CP-odd pseudo-Goldstone bosons whose couplings to matter respect a shift symmetry, and which may also make up the cosmic dark matter (DM) density [1–3]. The ALP coupling to nuclei N , $g_{aNN}\partial_\mu a \bar{N}\gamma^\mu\gamma^5 N$, reduces in the non-relativistic limit to a Hamiltonian $\gamma\vec{B}_a \cdot \vec{\sigma}_N$, where

$$\vec{B}_a = \frac{g_{aNN}}{\gamma}\nabla a \simeq g_{aNN}\frac{\sqrt{2\rho_{\text{DM}}}}{\gamma}\cos(\omega_a t)\vec{v}_a \quad (1)$$

acts as an effective oscillating magnetic field which couples to nuclear spins [4]. Here $\vec{v}_a \sim 10^{-3}c$ is the DM velocity (in what follows we will set $c = 1$), $\omega_a = m_a(1 + \mathcal{O}(v_a^2))$ with m_a the axion mass, $\rho_{\text{DM}} = 0.3 \text{ GeV/cm}^3$ is the DM density, and γ is the gyromagnetic ratio of N . Because \vec{B}_a is proportional to the DM velocity, this interaction is known as the “axion wind.” For QCD axions which could resolve the strong CP problem [5–8], $g_{aNN} \approx 3 \times 10^{-8} \text{ GeV}^{-1}(m_a/\text{eV})$ [9], yielding

$$|\vec{B}_a|_{\text{QCD}} \simeq 5 \times 10^{-23} \text{ T} \left(\frac{m_a}{10^{-7} \text{ eV}} \right) \quad (2)$$

taking $\gamma = 0.69 \text{ GeV}^{-1}$ ($\gamma/(2\pi) = 32.43 \text{ MHz/T}$) for the gyromagnetic ratio of ³He. Several experiments are aiming to detect the axion wind, including CASPEr-Wind [10–12] and CASPEr-ZULF [13, 14], which use a polarized sample of nuclear spins as the detection medium; comagnetometers using two species of spins to reduce noise [15, 16]; and QUAX, which uses polarized electron spins [17] (see Refs. [18, 19] for a review of other experimental approaches). In a close analogy to nuclear magnetic resonance (NMR), when an external B -field is tuned such that the sample Larmor frequency matches m_a , the spins will tip away from the external field, yielding a transverse magnetic field proportional to B_a which

grows linearly with time up to the axion coherence time, $\tau_a \simeq 2\pi/(m_a v_a^2)$ as long as this is larger than the spin relaxation time.

In this Letter, we describe a new detection mechanism which converts the small amplitude ALP signal into a small *frequency* shift in a large-amplitude NMR signal, allowing the use of precision frequency metrology to evade amplitude noise. The sample is an unusual phase of superfluid ³He, the homogeneous precession domain (HPD), which may be understood as a Bose-Einstein condensate (BEC) of spin-1 magnons formed by Cooper pairs of the spin-1/2 helium nuclei in the B-phase of the superfluid [20]. We will first review the properties of the HPD (based largely on the review [20]), then describe the effect of the axion wind, and finally estimate the sensitivity of the setup to various ALP masses and couplings.

HPD REVIEW

³He is a Fermi liquid which forms a superfluid below temperatures of $\sim 1 \text{ K}$; the excitations of this superfluid are spin-1 magnons. When a static magnetic field $\vec{B}_0 = B_0(z)\hat{z}$ is applied, the equilibrium magnetization is $\vec{M} = \chi\vec{B}_0$, where $\chi \sim 10^{-7}$ is the susceptibility which reaches a maximum at a temperature of 2.5 mK and pressures of 34 bar [21]. A transverse magnetic field pulse will torque the spins, injecting some number of spin-1 quanta (i.e. magnons), N_M . In the B-phase of ³He, the HPD is formed by the Bose condensation of these magnons after an RF pulse: a macroscopic fraction of the sample will spontaneously begin to precess coherently about \vec{B}_0 with the nuclear spins tipped at the Leggett angle, $\beta_0 = \cos^{-1}(-1/4) \approx 104^\circ$ (originating from dipole-dipole interactions), while the rest of the sample remains relaxed

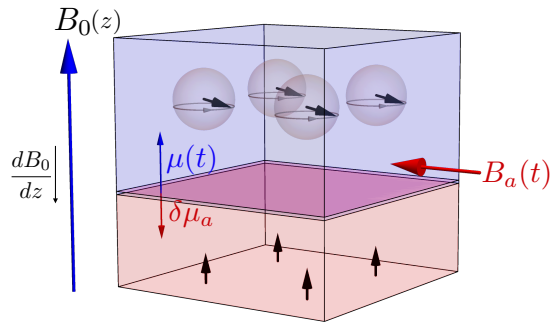


FIG. 1. Spins in the HPD (blue) precess at the local Larmor frequency set by the location of the DW, while the remainder of the sample (red) is relaxed. A transverse axion wind B_a acts as a small chemical potential $\delta\mu_a$ for magnons.

in equilibrium [22]. This is illustrated in Fig. 1: the HPD occupies a volume $V_{\text{HPD}} = N_M/n_M$, where

$$n_M = \frac{\chi B_0}{\gamma} (1 - \cos \beta_0) = \frac{5}{4} \frac{\chi B_0}{\gamma} \quad (3)$$

is the constant magnon density.

A striking feature of the HPD is that the precession frequency is spontaneously determined. One can view the HPD as a thermodynamic system at fixed particle number N_M , where the chemical potential μ is set by minimizing the free energy F . In fact, μ is the *local* Larmor frequency, corresponding to an angular precession frequency $\omega_L(z) = \gamma B_0(z)$, at the location z of the domain wall (DW) separating the HPD from the relaxed domain [23]. Thus, even in the presence of a spatially-varying B_0 , the entire HPD precesses coherently at the *same* frequency. In a lossless system, the precession would continue indefinitely at the frequency established at HPD formation, but due to longitudinal spin relaxation from surface and volume losses on a timescale T_1 , N_M will decrease monotonically [24]. For sufficiently large T_1 compared to the spin supercurrent propagation time, the HPD will continuously minimize F at a smaller V_{HPD} , and thus the precession frequency $\omega_L(t)$ will sweep through the local Larmor frequencies corresponding to the motion $z(t)$ of the DW, at a speed governed by T_1 . F is minimized when the HPD occupies the region of smaller B -field, so for dB_0/dz of definite sign, $\omega_L(t)$ will decrease monotonically and approximately linearly on timescales much shorter than T_1 . While the maximum attainable T_1 for the HPD is presently unknown, in the low-temperature limit magnetic modes in ^3He have exhibited T_1 as long as 1000 seconds [25, 26]. The B-phase is destabilized for $B_0 \gtrsim 0.55$ T [27], which sets the maximum ω_L of the HPD.

The aforementioned properties of the HPD may be understood through an effective description of the sample magnetization as described by the Bloch equations. With a static external magnetic field $\vec{B} = B_0(z)\hat{z}$ (not necessarily homogeneous) the magnetization \vec{M} in the HPD

evolves as

$$\frac{dM_z}{dt} = \frac{i\gamma}{2} (M_{xy}\bar{B}_{xy} - \bar{M}_{xy}B_{xy}) - \frac{M_z - \widetilde{M}_0}{5T_1}, \quad (4)$$

$$\frac{dM_{xy}}{dt} = -i\gamma (M_{xy}B_z - M_zB_{xy}) - \frac{M_{xy}}{T_1}, \quad (5)$$

where \widetilde{M}_0 is the equilibrium magnetization in the HPD, $M_{xy} \equiv M_x + iM_y$ is the transverse magnetization, $\bar{M}_{xy} = M_x - iM_y$, and likewise for B_{xy} and \bar{B}_{xy} . The factor of $5 = \frac{\cos \beta_0 - 1}{\cos \beta_0}$ in T_1 has been introduced for later convenience; note that the transverse and longitudinal relaxation times are not independent because these components of the magnetization are locked together by the spin supercurrents at the constant tip angle β_0 [28].

Since the magnetization in the relaxed domain does not evolve, we can treat the equilibrium magnetization as belonging to the HPD only via $\widetilde{M}_0 = \chi B_0 \mathbb{F}$, where \mathbb{F} is the HPD fraction of the sample. We parameterize $M_z = \chi B_0 \mathbb{F} \cos \beta_0$ and $M_{xy} = \chi B_0 \mathbb{F} \sin \beta_0 e^{-i\theta}$, which are time-dependent through the HPD fraction $\mathbb{F}(t)$ and because B_0 is evaluated at the position $z(t)$ of the domain wall. Suppose first that there is no transverse magnetic field, $B_{xy} = 0$. For homogeneous B_0 , Eq. (4) yields

$$\mathbb{F}(t) = \mathbb{F}_0 e^{-t/T_1}, \quad (6)$$

so the HPD fraction decays exponentially from its initial value \mathbb{F}_0 due to relaxation. Similarly, Eq. (5) yields

$$\dot{\theta} = \gamma B_0, \quad (7)$$

so that precession occurs at the local Larmor frequency $\omega_L = \gamma B_0$.

Due to the DW motion, if the external magnetic field is inhomogeneous, B_0 in Eq. (7) will acquire an effective time dependence, and thus so will ω_L . To see this, consider the evolution of the HPD over a short time interval $t \ll T_1$. For a fixed cross-sectional area A of the sample container of volume V , the position of the domain wall is $z(t) = -h\mathbb{F}(t)$, where $h = V/A$ is the height of the container and we have set $z = 0$ at the top of the container. At $t = 0$ we have $z_0 = -h\mathbb{F}_0$. For short times $t \ll T_1$, the DW position is

$$z(t) = -h\mathbb{F}_0 e^{-t/T_1} \approx z_0 + v_D t, \quad (8)$$

where $v_D \equiv h\mathbb{F}_0/T_1 = |z_0|/T_1$ is the instantaneous DW velocity at the height z_0 . Now, since the HPD precesses according to the magnetic field $B_0(z)$ at the DW, we Taylor-expand

$$B_0(z) \approx B_0(z_0) + \nabla_z B_0|_{z_0} (z - z_0) \equiv B_0(1 + \alpha v_D t), \quad (9)$$

where we have defined $\alpha \equiv \nabla_z B_0/B_0|_{z_0}$ as a tuneable parameter of the experiment. For the geometry defined in Fig. 1, $\alpha < 0$, and α can be taken to be constant in the region $z \approx z_0$. We further require $|\alpha(z - z_0)| \ll 1$ so that

n_M is approximately constant. Combining Eqs. (6) and (7) and expanding to first order in t/T_1 , the transverse magnetization is

$$M_{xy}(t \ll T_1) = M_{xy}(0) \left(1 - \frac{t}{T_1}\right) e^{-i\omega_L^0(1+\alpha v_D t/2)t}, \quad (10)$$

where $\omega_L^0 = \gamma B_0(z_0)$. The linear downward drift of the precession frequency, $\dot{\omega}_L \equiv \dot{\theta}(t) = \alpha v_D \omega_L^0 < 0$, is the key feature of the HPD.

EFFECT OF THE AXION WIND ON THE HPD

The effect of the axion wind on the HPD evolution can be directly computed by including \vec{B}_a as a source in the Bloch equations. We will first describe the effect qualitatively and estimate its parametric size, and then confirm this behavior with numerical simulations in the following section.

In CASPER, Larmor resonance is achieved when $\gamma B_0 = m_a$, and B_a generates a tip angle $\delta\beta(t) = \gamma B_a t$ that grows linearly with time up to $\min[\tau_a, T_2^*]$ where T_2^* is the dephasing time. The three principal challenges in this setup are (i) detecting the extremely small transverse field generated by $\delta\beta$; (ii) tuning B_0 in steps of $\sim 10^{-6}$ to achieve resonance at each possible axion mass, given the axion bandwidth $m_a v_a^2 \sim 10^{-6} m_a$; and (iii) generating a uniform B_0 to ensure that nearby spins do not dephase, thus preserving $T_2^* > \tau_a$. The HPD setup naturally sidesteps all of these challenges, as follows. Because the HPD is a macroscopic quantum state, the inhomogeneous B -field, which generates the linear frequency drift, preserves the precession phase in a macroscopic volume while scanning Larmor frequencies. This allows the HPD to probe many axion masses with the same field profile B_0 . In the HPD, the tip angle is fixed, so the torque from a transverse B_a instead resonantly changes the number of magnons in the BEC when the local Larmor frequency is equal to m_a , $|\Delta N_a| \simeq \chi B_0 B_a V_{\text{HPD}} \tau_a$. The axion wind can thus be seen as a small chemical potential $\delta\mu_a$ for magnons, as shown in Fig. 1. Since the magnon density in the BEC remains constant, V_{HPD} changes with ΔN_a , and hence the DW position shifts by an amount $|\Delta z| \simeq \gamma B_a |z_0| \tau_a$. This leads to a frequency shift,

$$\begin{aligned} \left| \frac{\Delta\omega_a}{\omega_L^0} \right| &\simeq (\gamma B_a)(\alpha z_0) \tau_a \\ &\approx 3 \times 10^{-13} \left(\frac{g_a N N}{10^{-10} \text{ GeV}^{-1}} \right) \left(\frac{\alpha z_0}{0.02} \right) \left(\frac{10^{-7} \text{ eV}}{m_a} \right). \end{aligned} \quad (11)$$

Note that since $B_a \propto m_a$ along the QCD line, the QCD axion frequency shift is independent of the mass:

$$\left(\left| \frac{\Delta\omega_a}{\omega_L^0} \right| \right)_{\text{QCD}} \approx 10^{-17} \left(\frac{\alpha z_0}{0.02} \right). \quad (12)$$

While Eq. (12) is a very small frequency shift, it is comparable to the best sensitivity currently achieved by microwave atomic clocks [29], and could thus be detected in principle with homodyne detection of the NMR signal referenced to a local oscillator. In contrast to CASPER, the overall amplitude of the NMR signal from the HPD is large, of order $M_{xy}(0) \sim \chi B_0$, with the smallness of the axion signal appearing in the frequency rather than the amplitude.

The resonance can persist while the DW sweeps through a frequency bandwidth up to the axion bandwidth, giving a resonance timescale

$$t_r \approx \frac{10^{-6} m_a}{|\dot{\omega}_L|} \sim \frac{10^{-6}}{\alpha z_0} T_1. \quad (13)$$

Define α^* such that $t_r = \tau_a$, e.g.

$$\alpha^* z_0 \simeq 0.02 \left(\frac{T_1}{1000 \text{ sec}} \right) \left(\frac{m_a}{10^{-7} \text{ eV}} \right). \quad (14)$$

Thus, depending on the choice of α ,

$$\left| \frac{\Delta\omega_a}{\omega_L^0} \right| \simeq (\gamma B_a)(\alpha z_0) \begin{cases} t_r, & t_r \leq \tau_a \ (\alpha \geq \alpha^*), \\ \sqrt{t_r \tau_a}, & t_r \geq \tau_a \ (\alpha \leq \alpha^*). \end{cases} \quad (15)$$

The scaling with $\sqrt{t_r}$ is a typical feature of measurements exceeding the coherence time and arises from adding in quadrature the incoherent frequency shifts in each interval τ_a [30]. The signal is maximized when $\alpha = \alpha^*$, which recovers Eqs. (11) and (12), but choosing larger α allows more axion masses to be scanned.

We can confirm the estimate in Eq. (11) with a perturbative analysis of the Bloch equations. Taking a transverse monochromatic axion field, $B_x = B_a \cos(m_a t + \phi)$, and writing $\mathbb{F} = \mathbb{F}^{(0)}(1 + \mathbb{F}^{(1)})$ where $\mathbb{F}^{(0)}$ is the solution of Eq. (6) and $\mathbb{F}^{(1)}$ is proportional to B_a , we have for $t \ll T_1$ and to leading order in B_a ,

$$\frac{d\mathbb{F}^{(1)}}{dt} \approx -\tan \beta_0 \gamma B_a \cos(m_a t + \phi) \sin(-\omega_L(t)t). \quad (16)$$

On resonance when $m_a = \omega_L(t)$, the right-hand side contains a constant term $\frac{1}{2} \sin \phi$, and thus the solution for $\mathbb{F}^{(1)}$ is

$$\mathbb{F}^{(1)}(t) \approx - \left(\frac{1}{2} \sin \phi \right) (\gamma B_a \tan \beta_0) t \quad (17)$$

which grows linearly with time. In fact, integrating Eq. (16) we can obtain an analytic solution valid for $t \ll T_1$,

$$\mathbb{F}^{(1)}(t) \approx \left(\frac{-\tan \beta_0 \gamma B_a}{2} \right) \frac{\cos \phi S(\Omega t) + \sin \phi C(\Omega t)}{\Omega}, \quad (18)$$

where $\Omega \equiv \sqrt{\frac{\alpha z_0 \omega_L^0}{\pi T_1}}$ and $S(x)$ and $C(x)$ are the Fresnel sine and cosine integrals, respectively.

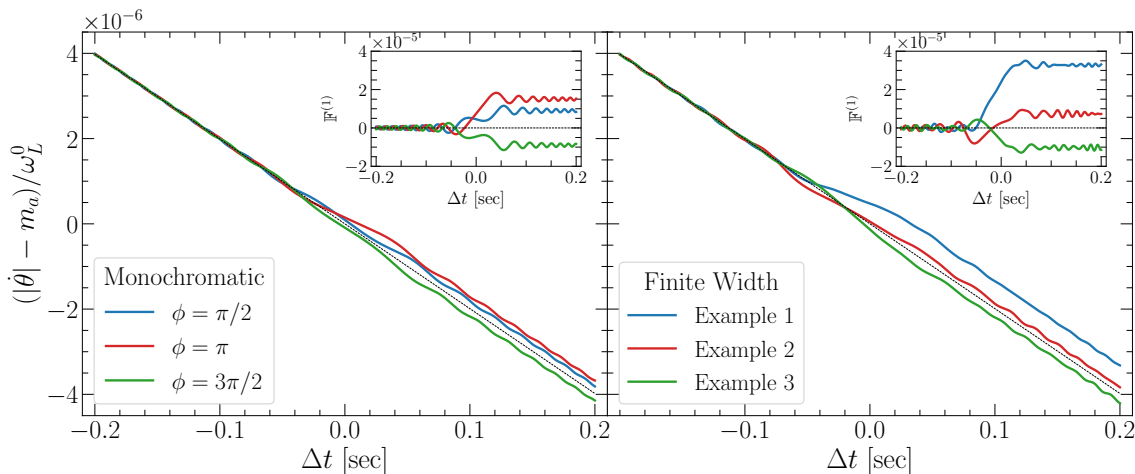


FIG. 2. The fractional HPD frequency shift $(|\dot{\theta}| - m_a)/\omega_L^0$ (inset: first-order HPD fraction $\mathbb{F}^{(1)}$) near resonance, with $g_{aNN} = 5 \times 10^{-5} \text{ GeV}^{-1}$, $B_0 = 0.55 \text{ T}$ ($m_a \approx 7 \times 10^{-8} \text{ eV}$), $\alpha_{z0} \simeq 0.02$, and $T_1 = 1000 \text{ sec}$. The axion coupling is taken to be artificially large for illustration purposes to render the frequency shift visible. The resonance occurs at $\Delta t = 0$, and $t_r = \tau_a = 0.05 \text{ s}$, and \vec{B}_a is assumed to be transverse. The grey dashed lines indicate the behavior in the absence of an axion resonance. **Left:** monochromatic axion field $\vec{B}_a(t) = \frac{g_{aNN}\sqrt{2\rho_{\text{DM}}}}{\gamma}\vec{v}_0 \cos(m_a t + \phi)$ for three choices of ϕ . **Right:** three realizations of the stochastic axion field $\vec{B}_a(t)$ given by Eq. (19).

The effect of the axion can be interpreted as a first-order contribution to the DW velocity $\Delta v_D = -(\frac{1}{2} \sin \phi) z_0 \tan \beta_0 \gamma B_a$, which then feeds back into the precession frequency because $z - z_0 = h\mathbb{F}_0 - h\mathbb{F}^{(0)}(1 + \mathbb{F}^{(1)}) \approx (v_D + \Delta v_D)t$. In other words, the first-order frequency shift is $\Delta\omega_a(t) = \omega_L^0 \alpha \Delta v_D t$, and integrating up to τ_a we recover the parametric estimate of Eq. (11), up to the $\mathcal{O}(1)$ factor $\frac{1}{2} \sin \phi \tan \beta_0$. There is also an additional first-order effect on the precession phase θ , but it is always parametrically smaller than the frequency shift induced from the variation of V_{HPD} . Finally, note that a longitudinal axion field, $B_z = B_a \cos(m_a t + \phi)$, will not yield a resonance but will rather imprint fast oscillations at frequency m_a on the phase θ .

SIMULATIONS, NOISE, AND SENSITIVITY

To validate the above analysis, we numerically solved the Bloch equations with an axion source, both for a monochromatic axion field and an axion field with the expected 10^{-6} bandwidth from the DM velocity dispersion. Since the axion field is a random field with a known power spectrum, for the latter case, we used the time-domain axion field constructed from sampling the speed distribution according to the prescription in Ref. [31]. Specifically, we took

$$\vec{B}_a = g_{aNN} \frac{\sqrt{2\rho_{\text{DM}}}}{\gamma} \vec{v}_0 \times \sum_j \alpha_j \sqrt{f(v_j)} \Delta v \cos(m_a (1 + v_j^2/2) t + \phi_j). \quad (19)$$

The sum is over groups of axion particles, each group having a speed $\in [v_j, v_j + \Delta v]$. Here α_j is a Rayleigh-distributed random variable, $\phi_j \in [0, 2\pi)$ is a random phase, and $f(v)$ is the local DM speed distribution which we take to be Maxwellian with dispersion $v_0 = 220 \text{ km/sec}$, boosted to the lab frame by $v_{\text{Earth}} = 232.24 \text{ km/sec}$. A key feature of the HPD setup is the possibility of observing daily modulation, since the same axion masses may be scanned multiple times throughout the day. However, for this analysis we fix \vec{v}_0 to be transverse and leave a full daily modulation analysis for future work. Indeed, we use the stochastic field simply to validate our treatment of the coherence time, and we expect that our parametric estimates of the signal strength will differ by $\mathcal{O}(1)$ factors from a full treatment of the correlated components of ∇a [32, 33].

Fig. 2 shows the evolving fractional frequency shift $(|\dot{\theta}(t)| - m_a)/\omega_L^0$ and the perturbation to the HPD fraction $\mathbb{F}^{(1)}(t)$, when a transverse axion wind is on resonance with the Larmor frequency. The DW can shift either up or down depending on the phase when the resonance occurs, and hence the frequency can shift above or below the linear drift indicated by the grey lines. As mentioned earlier, if the axion wind is longitudinal, no such resonance occurs. Both the monochromatic and the stochastic axion sources show the expected linear growth in $\mathbb{F}^{(1)}$ during the resonance (given by Eq. (18) in the case of the monochromatic axion). The accumulated frequency shift $\Delta\omega_a/\omega_L^0$ appears as a persistent offset at $\Delta t \gg t_r$ and matches our parametric estimates in Eq. (11).

To obtain a projected sensitivity for the HPD setup, we need to consider possible noise sources. Since we have already argued that the expected $\Delta\omega_a$ is (in principle)

within the sensitivity of state-of-the-art atomic clocks, we will focus on irreducible noise sources. Fortunately, the unique properties of the HPD makes thermal noise a negligible concern. Unlike the case of a BEC of atoms, thermal fluctuations in ^3He do not cause the number of magnons in the condensate to fluctuate, but rather affect the normal fluid component of the ^3He superfluid. Thus, thermal noise will not lead to a frequency shift.

In fact, the leading irreducible noise source is stochastic fluctuations in magnon number. Over a time interval $\Delta t \ll T_1$, losses reduce the average number of magnons by $N_{\text{loss}} = n_M \Delta V_{\text{HPD}}$, where $\Delta V_{\text{HPD}} = v_D A \Delta t$ is the change in HPD volume over Δt . This will lead to Poissonian “shot noise” of order $\sigma_N = \sqrt{N_{\text{loss}}}$, which will cause the HPD volume and hence the frequency to fluctuate. Taking $\Delta t = \tau_a$, the noise on the frequency shift is

$$\left| \frac{\Delta\omega_{\text{stoch.}}}{\omega_L^0} \right| = 7 \times 10^{-15} \times \left(\frac{\alpha z_0}{0.02} \right) \left(\frac{10^3 \text{ s}}{T_1} \right)^{1/2} \left(\frac{10^{-7} \text{ eV}}{m_a} \right) \left(\frac{100 \text{ cm}^3}{V_{\text{HPD}}} \right)^{1/2}. \quad (20)$$

We leave the precise microscopic characterization of the stochastic noise to future work, including an analysis of surface and volume loss mechanisms, but we note that the quantized fluctuation of magnons in the HPD as parameterized by T_1 is a reasonable coarse-grained characterization of many such microphysical phenomena.

Since the Larmor frequency continuously changes in the experiment, the number of axion resonances covered in a single run is given by roughly $T_1/t_r \sim 10^6(\alpha z_0)$, where t_r is given by Eq. (13). Repeating the experiment \mathcal{N} times suppresses the noise by $\sqrt{\mathcal{N}}$. However, since the axion field is incoherent between the different runs, the signal-to-noise ratio $\text{SNR} \equiv \left| \frac{\Delta\omega_a}{\Delta\omega_{\text{stoch.}}} \right|$ scales as $\mathcal{N}^{1/4}$ for the same reasons as discussed in Eq. (15). Letting $\mathcal{N} = t_{\text{int}}/T_1$ where t_{int} is the total integration time, we have

$$\text{SNR} \approx \gamma B_a \sqrt{V_{\text{HPD}} n_M} (T_1 t_{\text{int}})^{1/4} \times \min[\sqrt{t_r}, \sqrt{\tau_a}]. \quad (21)$$

Choosing $t_r = \tau_a$ for the maximum sensitivity gives

$$\text{SNR}_{\text{QCD}} \approx 0.03 \left(\frac{V_{\text{HPD}}}{100 \text{ cm}^3} \right)^{1/2} \left(\frac{T_1}{10^3 \text{ s}} \right)^{1/4} \left(\frac{t_{\text{int}}}{1 \text{ yr}} \right)^{1/4} \times \left(\frac{m_a}{7 \times 10^{-8} \text{ eV}} \right) \quad (22)$$

for couplings on the QCD line; the axion mass $m_a = 7 \times 10^{-8} \text{ eV}$ is the largest mass which can be probed before the HPD destabilizes at large fields.

Fig. 3 shows a projected sensitivity on g_{aNN} taking $\text{SNR} = 1$. Also shown are the star cooling bounds (green) from SN 1987A [34] and neutron stars [35] (assuming an

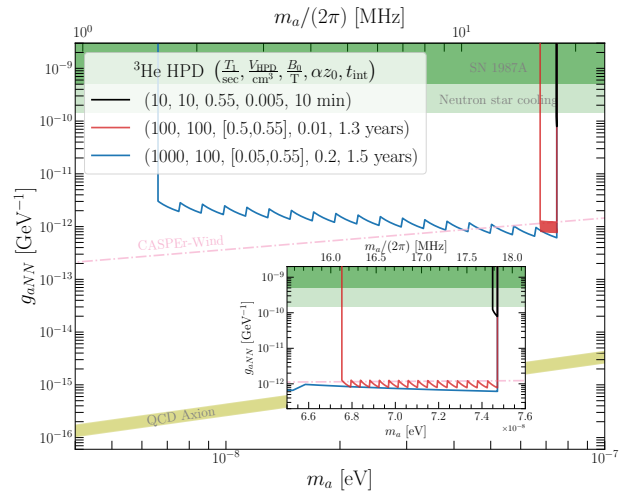


FIG. 3. Projected sensitivity to g_{aNN} ($\text{SNR} = 1$) from the ^3He HPD (black, red, blue), for various choices of parameters. The green shaded regions correspond to the star cooling bounds from SN 1987A [34], and neutron stars [35] (assuming an axion-neutron coupling). The dashed red lines are the CASPER-Wind projections from Ref. [11].

axion-neutron coupling), as well as the projected sensitivity (red) from CASPER-Wind [11]. As anticipated, choosing a large gradient α results in a larger coverage in axion masses, at the cost of less time spent in each resonance and hence a smaller SNR. However, comparable sensitivity to CASPER-Wind over an order of magnitude in m_a can be achieved with reasonable parameters in 1.5 years of measurement time at 1 month per B -field tune.

CONCLUSIONS

In this Letter we have described a new proposed experiment for detection of the axion wind which exploits the macroscopic coherent properties of the B-phase of ^3He . In future work we plan to further improve the projected sensitivity by taking into account the correlations between the \mathcal{N} measurements induced by daily modulation, as well as correlations between spatially-separated samples [36], which may increase the SNR such that QCD axion detection at masses $\simeq 10^{-7} \text{ eV}$ is possible. We close by emphasizing that even without further improvements to T_1 beyond those already achieved in the laboratory (black curve in Fig. 3) the HPD detection scheme could achieve world-leading limits on the axion wind coupling which exceed the most stringent astrophysical bounds.

Acknowledgments. We thank Doug Beck, Andrei Derevianko, Vladimir Eltsov, Jeff Filippini, Joshua Foster, Elizabeth Goldschmidt, Tony Leggett, David J.E. Marsh, Nicholas Rodd, Benjamin Safdi, James Sauls, Ilya Sochnikov, Tomer Volansky, and Kathryn Zurek for helpful discussions. We thank Rachel Nguyen for assistance with implementation of the time-domain axion field, and Yiming Zhong for artistic assistance. We especially thank

Andrew Geraci for facilitating collaboration which led to many of the ideas in this work. The work of YK and JSE is supported in part by DOE grant DE-SC0015655. CG acknowledges the Aspen Center for Physics for its hospitality where part of this work is done, which is supported by National Science Foundation grant PHY-1607611. CG is supported by the DOE QuantISED program through the theory consortium “Intersections of QIS and Theoretical Particle Physics” at Fermilab. WPH, MDN, and JWS acknowledge support from the NSF Division of Materials Research grant DMR-2210112.

-
- [1] J. Preskill, M. B. Wise, and F. Wilczek, Cosmology of the Invisible Axion, *Phys. Lett.* **120B**, 127 (1983).
- [2] L. F. Abbott and P. Sikivie, A Cosmological Bound on the Invisible Axion, *Phys. Lett.* **120B**, 133 (1983).
- [3] M. Dine and W. Fischler, The Not So Harmless Axion, *Phys. Lett.* **120B**, 137 (1983).
- [4] P. W. Graham and S. Rajendran, New Observables for Direct Detection of Axion Dark Matter, *Phys. Rev. D* **88**, 035023 (2013), arXiv:1306.6088 [hep-ph].
- [5] R. D. Peccei and H. R. Quinn, CP Conservation in the Presence of Instantons, *Phys. Rev. Lett.* **38**, 1440 (1977).
- [6] R. D. Peccei and H. R. Quinn, Constraints Imposed by CP Conservation in the Presence of Instantons, *Phys. Rev.* **D16**, 1791 (1977).
- [7] S. Weinberg, A New Light Boson?, *Phys. Rev. Lett.* **40**, 223 (1978).
- [8] F. Wilczek, Problem of Strong p and t Invariance in the Presence of Instantons, *Phys. Rev. Lett.* **40**, 279 (1978).
- [9] G. Grilli di Cortona, E. Hardy, J. Pardo Vega, and G. Villadoro, The QCD axion, precisely, *JHEP* **01**, 034, arXiv:1511.02867 [hep-ph].
- [10] A. Garcon *et al.*, The Cosmic Axion Spin Precession Experiment (CASPER): a dark-matter search with nuclear magnetic resonance 10.1088/2058-9565/aa9861 (2017), arXiv:1707.05312 [physics.ins-det].
- [11] D. F. Jackson Kimball *et al.*, Overview of the Cosmic Axion Spin Precession Experiment (CASPER), *Springer Proc. Phys.* **245**, 105 (2020), arXiv:1711.08999 [physics.ins-det].
- [12] D. Aybas *et al.*, Search for Axionlike Dark Matter Using Solid-State Nuclear Magnetic Resonance, *Phys. Rev. Lett.* **126**, 141802 (2021), arXiv:2101.01241 [hep-ex].
- [13] T. Wu *et al.*, Search for Axionlike Dark Matter with a Liquid-State Nuclear Spin Comagnetometer, *Phys. Rev. Lett.* **122**, 191302 (2019), arXiv:1901.10843 [hep-ex].
- [14] A. Garcon, J. W. Blanchard, G. P. Centers, N. L. Figueroa, P. W. Graham, D. F. J. Kimball, S. Rajendran, A. O. Sushkov, Y. V. Stadnik, A. Wickenbrock, T. Wu, and D. Budker, Constraints on bosonic dark matter from ultralow-field nuclear magnetic resonance, *Science Advances* **5**, 10.1126/sciadv.aax4539 (2019).
- [15] I. M. Bloch, G. Ronen, R. Shaham, O. Katz, T. Volansky, and O. Katz (NASDUCK), New constraints on axion-like dark matter using a Floquet quantum detector, *Sci. Adv.* **8**, abl8919 (2022), arXiv:2105.04603 [hep-ph].
- [16] J. Lee, M. Lisanti, W. A. Terrano, and M. Romalis, Laboratory Constraints on the Neutron-Spin Coupling of feV-scale Axions, (2022), arXiv:2209.03289 [hep-ph].
- [17] N. Crescini *et al.* (QUAX), Axion search with a quantum-limited ferromagnetic haloscope, *Phys. Rev. Lett.* **124**, 171801 (2020), arXiv:2001.08940 [hep-ex].
- [18] I. G. Irastorza and J. Redondo, New experimental approaches in the search for axion-like particles, *Prog. Part. Nucl. Phys.* **102**, 89 (2018), arXiv:1801.08127 [hep-ph].
- [19] C. B. Adams *et al.*, Axion Dark Matter, in *2022 Snowmass Summer Study* (2022) arXiv:2203.14923 [hep-ex].
- [20] Y. M. Bunkov and G. E. Volovik, Spin superfluidity and magnon bec (2012), arXiv:1003.4889 [cond-mat.other].
- [21] J. C. Wheatley, Experimental properties of superfluid ^3He , *Reviews of Modern Physics* **47**, 415 (1975).
- [22] I. Fomin, Long-lived induction signal and spatially nonuniform spin precession in $^3\text{He-B}$, *JETP Lett* **40** (1984).
- [23] Y. M. Bunkov and G. E. Volovik, Bose-einstein condensation of magnons in superfluid ^3He , *J Low Temp Phys* **150**, 135 (2008), number: 3-4.
- [24] I. A. Fomin, Separation of magnetization precession in $^3\text{He-B}$ into two magnetic domains. (theory), in *World Scientific Series in 20th Century Physics*, Vol. 11 (WORLD SCIENTIFIC, 1996) pp. 251–257.
- [25] D. Geller and D. Lee, Stabilization of homogeneously precessing domains by large magnetic fields in superfluid $^3\text{He-B}$, *Physical Review Letters* **85**, 1032 (2000).
- [26] S. N. Fisher, A. Guénault, A. Hale, G. R. Pickett, P. Reeves, and G. Tvalashvili, Thirty-minute coherence in free induction decay signals in superfluid $^3\text{He-B}$, *Journal of low temperature physics* **121**, 303 (2000).
- [27] H. N. Scholz, *Magnetic Properties of Superfluid and Normal Helium-3, and a Search for Superconductivity in Gold*, Ph.D. thesis, The Ohio State University (1981).
- [28] Y. M. Bunkov, Spin supercurrent and novel properties of NMR in ^3He , in *Progress in low temperature physics*, Vol. 14, edited by W. P. Halperin (Elsevier, 1995) Chap. 2, pp. 69–158.
- [29] T. Nakamura, J. Davila-Rodriguez, H. Leopardi, J. A. Sherman, T. M. Fortier, X. Xie, J. C. Campbell, W. F. McGrew, X. Zhang, Y. S. Hassan, D. Nicolodi, K. Belay, A. D. Ludlow, S. A. Diddams, and F. Quinlan, Coherent optical clock down-conversion for microwave frequencies with 10^{-18} instability, *Science* **368**, 889 (2020), <https://www.science.org/doi/pdf/10.1126/science.abb2473>.
- [30] D. Budker, P. W. Graham, M. Ledbetter, S. Rajendran, and A. Sushkov, Proposal for a Cosmic Axion Spin Precession Experiment (CASPER), *Phys. Rev. X* **4**, 021030 (2014), arXiv:1306.6089 [hep-ph].
- [31] J. W. Foster, N. L. Rodd, and B. R. Safdi, Revealing the Dark Matter Halo with Axion Direct Detection, *Phys. Rev. D* **97**, 123006 (2018), arXiv:1711.10489 [astro-ph.CO].
- [32] M. Lisanti, M. Moschella, and W. Terrano, Stochastic properties of ultralight scalar field gradients, *Phys. Rev. D* **104**, 055037 (2021), arXiv:2107.10260 [astro-ph.CO].
- [33] A. V. Gramolin, A. Wickenbrock, D. Aybas, H. Bekker, D. Budker, G. P. Centers, N. L. Figueroa, D. F. J. Kimball, and A. O. Sushkov, Spectral signatures of axionlike dark matter, *Phys. Rev. D* **105**, 035029 (2022), arXiv:2107.11948 [hep-ph].
- [34] P. Carezza, T. Fischer, M. Giannotti, G. Guo, G. Martínez-Pinedo, and A. Mirizzi, Improved axion emissivity from a supernova via nucleon-nucleon bremsstrahlung, *Journal of Cosmology and Astroparticle Physics* **2019** (10), 016.

- [35] M. V. Beznogov, E. Rrapaj, D. Page, and S. Reddy, Constraints on axion-like particles and nucleon pairing in dense matter from the hot neutron star in HESS j1731-347, *Physical Review C* **98**, 10.1103/physrevc.98.035802 (2018).
- [36] J. W. Foster, Y. Kahn, R. Nguyen, N. L. Rodd, and B. R. Safdi, Dark Matter Interferometry, *Phys. Rev. D* **103**, 076018 (2021), arXiv:2009.14201 [hep-ph].